JOURNAL OF AIRCRAFT
Vol. 33, No. 1, January–February 1995

Buffeting of a Fin: Streamwise Evolution of Flow Structure

S. Canbazoglu,* J.-C. Lin,† S. Wolfe,‡ and D. Rockwell§
Lehigh University, Bethlehem, Pennsylvania 18015

The encounter of a broken-down vortex with a fin is characterized using high-image-density particle image velocimetry, which provides instantaneous and averaged representations of the distorted flow structure. Averaged patterns of sectional streamlines and streamwise vorticity show well-defined, large-scale vortical motions having vorticity of the same orientation as, and counter to, the incident vortex. The countervortex, generated at the inclined leading edge of the fin, exhibits substantial values of vorticity and circulation. Corresponding instantaneous images show pronounced concentrations of streamwise vorticity, which can have peak vorticity levels and values of circulation that exceed the averaged values by factors of three to five. The location and form of these vorticity concentrations vary randomly with time.

Nomenclature

C = chord of delta wing
C_F = root chord of fin
M = magnification
R_ω = vorticity correlation function
t = time
t_F = thicknes of fin
t_s = thickness of strut
t_w = thickness of wing
U = freestream velocity
x_b = coordinate along axis of broken-down vortex measured from apex of wing
y = coordinate in plane of fin
z = coordinate perpendicular to surface of fin
α = angle of attack of delta wing
Δx = distance from onset of vortex breakdown to apex of fin measured
Λ = sweep angle of wing
ν = kinematic viscosity
ω = instantaneous vorticity
$\bar{\omega}$ = time-averaged vorticity
$\tilde{\omega}$ = vorticity fluctuation

I. Introduction

THE encounter of a streamwise vortex with the leading edge of a fin is expected to generate a highly distorted flow, which changes rapidly with streamwise distance along the surface of the fin. Development of the flow structure will be particularly complex when the incident vortex is in a broken-down state. Mayori and Rockwell[1] have demonstrated pronounced splitting of a broken-down vortex when it encounters a thin flat plate having a nonswept leading edge. In the event that the vortex encounters a fin with substantial leading-edge sweep, its distortion is expected to exhibit a number of distinctive features.

Several investigations have provided valuable qualitative insight into vortex–fin interaction. The cross-sectional form and position of a vortex incident upon a fin is characterized in the laser sheet–smoke visualization study of Shah,[2] who shows its sensitivity to the presence of a leading-edge extension (LEX) fence. Washburn et al.[3] schematically portray generation of a vortex of counter (opposite) sense, relative to that of the incident vortex. This countervortex emanated from the leading-edge region of the fin, which was located downstream of the trailing edge of a delta wing. Such buffeting phenomena are also important for missile-tip vortex–control surface interactions and, as demonstrated by Kiedaisch and Acharya,[4] varying degrees of symmetry and preservation or loss of coherence of the incident vortical structures are evident, depending upon the azimuthal orientation of the incident vortices relative to the leading edge of the control surface. Quantitative insight into the cross-sectional structure of a broken-down vortex approaching the vertical stabilizer of an F/A-18 is provided by the Doppler global velocimeter studies of Lee et al.[5] Their measurements of the mean and rms velocity fields suggest that the approach vortex is not chaotic.

It is, of course, expected that the induced surface pressure will be related to the quantitative distortion of the broken-down vortex past the fin. The wide variety of surface pressure and force measurements carried out to date are summarized in a companion manuscript by Canbazoglu et al.,[6] who interpret surface pressure in terms of quantitative flow parameters along the surface of the fin.

The aim of the present investigation is to determine the instantaneous, quantitative flow structure over the cross section of a broken-down vortex along a fin. By considering global representations of the flow across the vortex and comparing distributions of streamwise vorticity and sectional streamlines it will be possible to identify and quantitatively interpret the major features of the vortex–fin interaction. In doing so, it is insightful to base the averaged patterns of the flow on a succession of global, instantaneous states. This approach reveals the manner in which the large-scale vortical motion of the averaged flow acts with the concentrations of vorticity of the instantaneous flow to buffet the surface of the fin.

II. Experimental System and Techniques

Experiments were performed in a water channel having a cross section of 616 × 584 mm. The flow velocity was maintained at 147 mm/s. The delta wing had a sweep angle Λ = 75 deg, a thickness-to-chord ratio t_w/C = 0.0192, and a chord of 330 mm, giving a Reynolds number based on C of $Re = UC/\nu = 4.86 \times 10^4$. As indicated in Fig. 1 a fin was mounted

Received September 22, 1994; revision received May 29, 1995; accepted for publication June 15, 1995.

*Visiting Research Scientist, Department of Mechanical Engineering and Mechanics, 19 Memorial Drive West.
†Research Associate, Department of Mechanical Engineering and Mechanics, 19 Memorial Drive West.
‡Research Assistant, Department of Mechanical Engineering and Mechanics, 19 Memorial Drive West.
§Paul B. Reinhold Professor, Department of Mechanical Engineering and Mechanics, 19 Memorial Drive West. Senior Member AIAA.

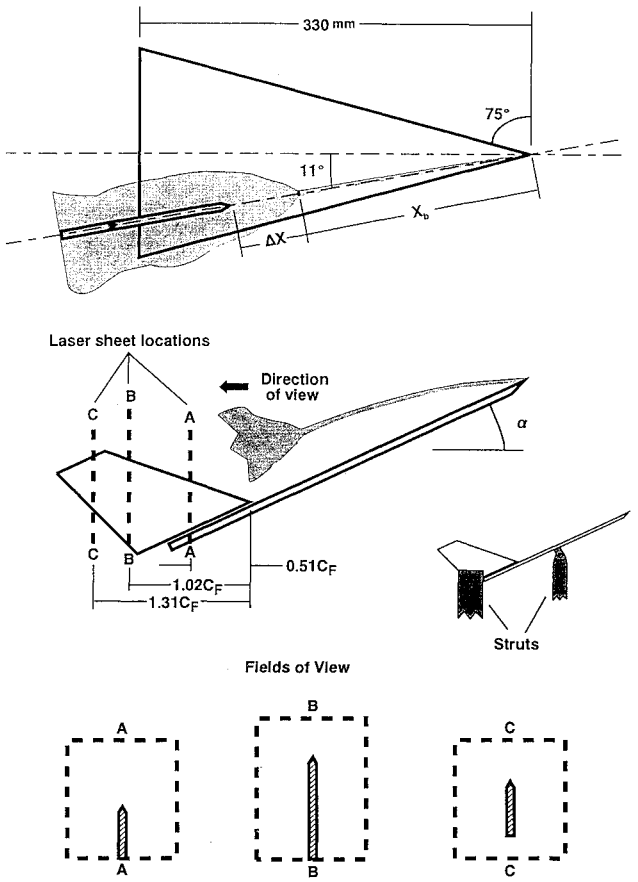

Fig. 1 Overview of delta wing–fin system.

on the delta wing in such a manner that it was aligned with the axis of the leading-edge vortex. The fin had a root chord C_F = 105 mm and a thickness-to-chord ratio t_F/C_F = 0.12. The leading edge and the tip edge of the fin were beveled symmetrically at an angle of 30 deg. The delta wing–fin system was mounted in an inverted position in the water channel, such that the wing was at a negative α, in order to facilitate laser diagnostics. The wing was held in position using the traditional technique of a thin strut extending vertically from the midchord of the wing up to the free surface. Likewise, the fin was supported independently with a streamlined strut extending up through the free surface and having a thickness t_s/C_F = 0.12. This inverted position of the wing allowed acquisition of instantaneous images of the velocity over the fields of view indicated in Fig. 1. These views corresponded to cuts A–A, B–B, and C–C and are referred to, respectively, as the leading, mid, and trailing regions of the fin. As indicated, these fields of view were defined by orienting the vertical laser sheet orthogonal to the plane of the fin. Vortex breakdown was found to occur at a nominal location x_b/C = 0.70. This corresponds to a distance $\Delta x/C$ = 0.06 upstream of the apex of the fin.

High-image-density particle image velocimetry (PIV) was employed to determine the instantaneous velocity field and corresponding vorticity contours and streamline patterns over an entire plane. This approach is centered on a laser scanning concept described in detail by Rockwell et al.,[7] Rockwell et al.,[8] and Rockwell and Lin.[9] A continuous wavelength argon-ion laser (3 W) provided the laser beam, which was transmitted through a series of conditioning optics and eventually impinged upon each successive facet of a 72-faceted rotating mirror, providing an effective scanning frequency of 630 Hz. The camera shutter was held open long enough to allow multiply exposed images to be recorded. A Nikon F-4 camera

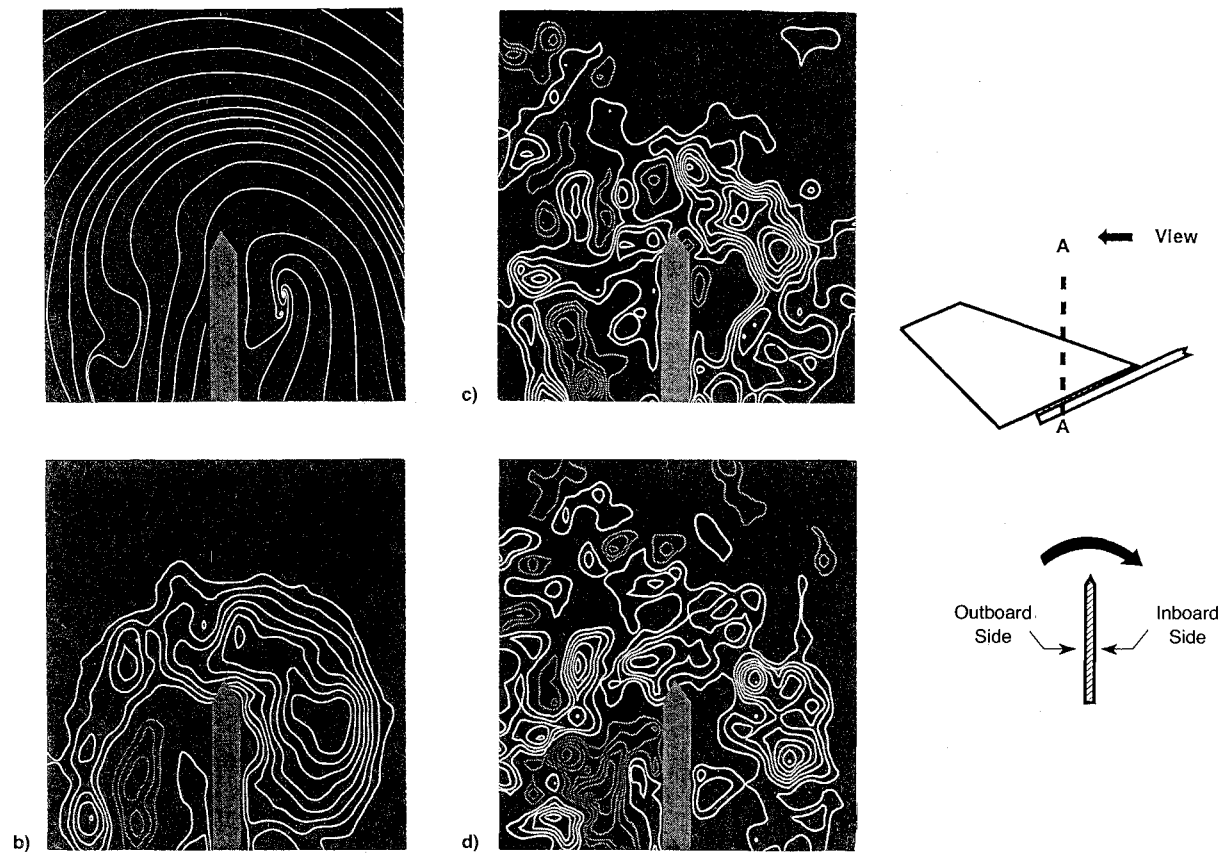

Fig. 2 Cross section of vortex–fin interaction in leading region of fin showing a) averaged streamlines, b) averaged vorticity contours, and c) and d) instantaneous vorticity contours. For averaged vorticity contours, minimum and incremental levels of vorticity are ±1.5 and 1 l/s, respectively; for instantaneous contours, ±2.5 and 2.5 l/s.

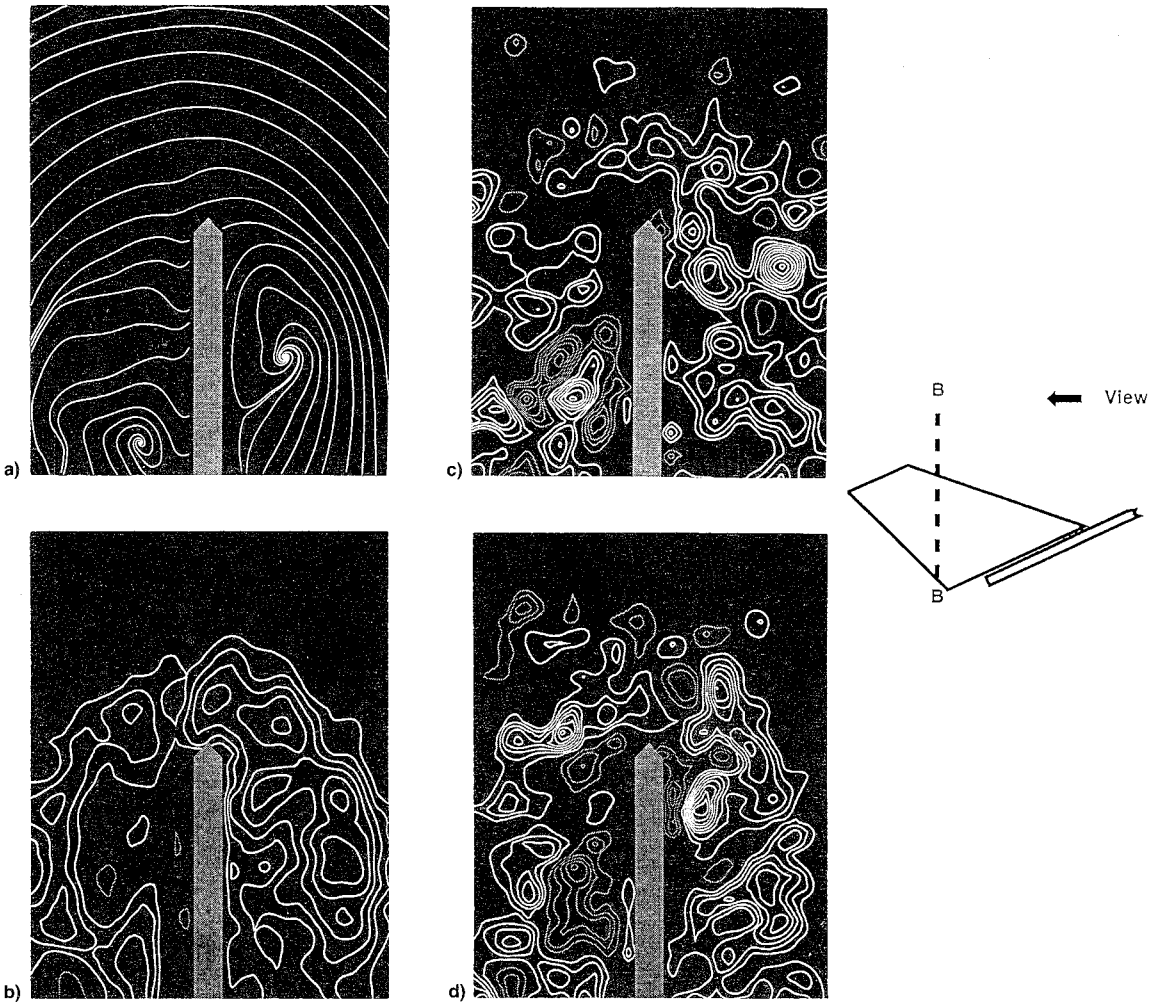

Fig. 3 Cross section of vortex–fin interaction in midregion of fin showing a) averaged streamlines, b) averaged vorticity contours, and c) and d) instantaneous vorticity contours. For averaged vorticity contours, minimum and incremental levels of vorticity are ±1.5 and 1 l/s, respectively; for instantaneous contours, ±2.5 and 2.5 l/s.

having a 105-mm lens with a magnification $M = 0.14$ was controlled by a laboratory microcomputer. The multiply exposed images were recorded on 35-mm high resolution Tmax Kodak film (400 ASA). Each negative was interrogated with a Nikon digitizer at a resolution of 125 pixels/mm. A single-frame, cross-correlation technique was employed to determine the field of 1500 velocity vectors. During the interrogation process, a square area of dimensions 0.8 × 0.8 mm was defined on the plane of the negative. This area corresponded, via the magnification factor $M = 0.14$, to an area in the plane of the laser sheet of 5.7 × 5.7 mm. Since an overlap of 50% was employed in order to satisfy the Nyquist criterion during the interrogation process, the effective grid size in the plane of the laser sheet was $\Delta l/M = 2.86$ mm.

In all cases, averaged images were obtained by averaging the velocity from 20 images acquired at a time spacing much longer than the convective time scale C/U, i.e., at $5C/U = 11.2$ s. This time spacing ensures that repetitive events do not influence the averaging process.

III. Evolution of Averaged and Instantaneous Flow Structure

Figures 2–4 show averaged and instantaneous representations of streamlines and contours of constant vorticity at three representative locations: 1) in the leading region of the fin, 2) at the midregion, and 3) in the trailing region. Taken together, these representations show the streamwise evolution of vorticity concentrations having the same sense as, and counter to, the streamlines of the primary vortex formed from the leading edge of the wing.

A. Leading Region of Fin

The averaged streamline pattern of Fig. 2a exhibits a generally clockwise motion above the apex of the fin. On the inboard (right) side of the fin, a spiral occurs within the region defined by the separation streamline from the apex (upper tip) of the fin; in this region, the streamlines swirl outward. On the outboard (left) side, the streamlines are substantially distorted, suggesting the existence of a secondary vortex. The patterns of vorticity corresponding to these averaged streamlines are given in Fig. 2b. On the inboard side, there is a single large-scale vortex defined by a single extremum of vorticity. On the outboard side, however, the structure is more complex. Within the region of positive (white) vorticity representing the separating shear layer, there is a well-defined concentration of negative (gray) vorticity, indicating the existence of a countervortex. Generation of a countervortex has been observed by Washburn et al.[3] using qualitative visualization of the crossflow past a fin having a highly swept leading edge, with the apex of the fin located at the trailing edge of the delta wing, in contrast to the present geometry, where it is upstream of the trailing edge. In their case, the center of the vortex encountering the leading edge of the fin is at a substantially higher elevation. Although the mechanism of initial formation of the counter- (tail) vortex in their case appears similar, it rapidly rises above the tip of the tail and

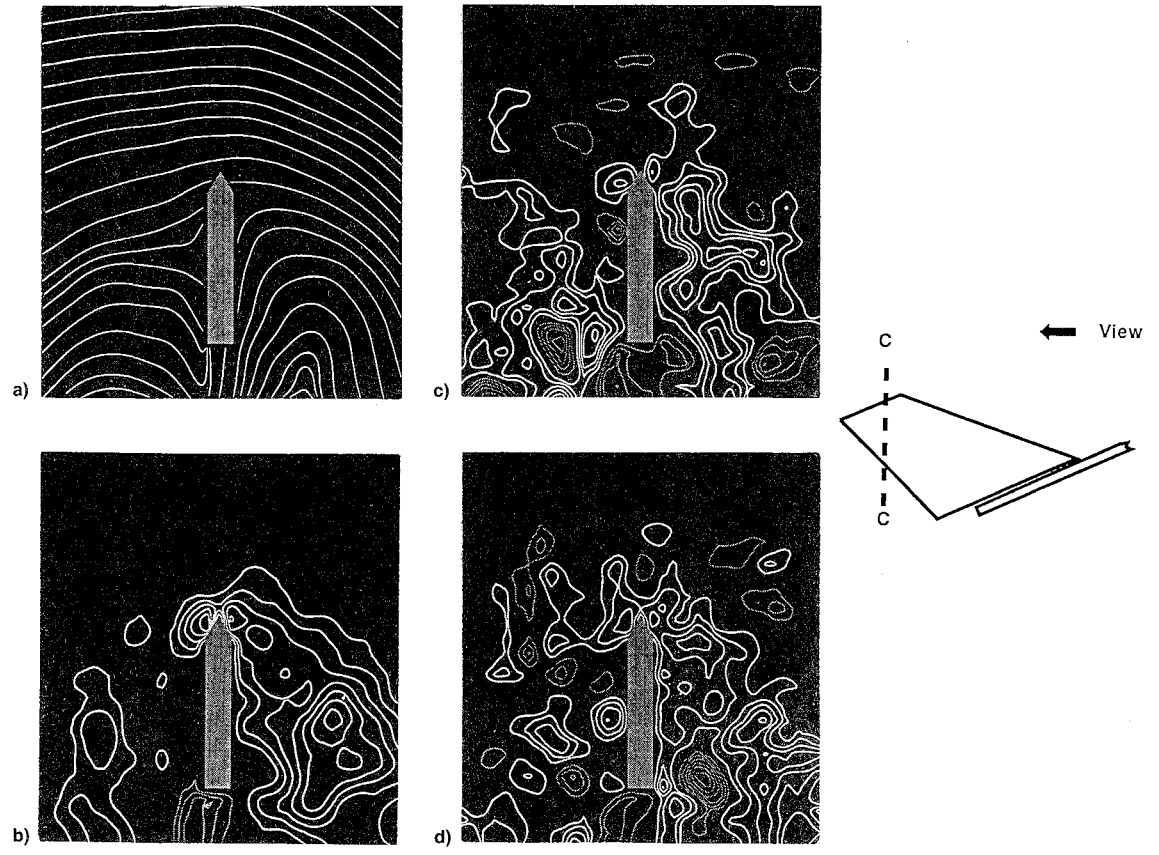

Fig. 4 Cross section of vortex–fin interaction in trailing region of fin showing a) averaged streamlines, b) averaged vorticity contours, and c) and d) instantaneous vorticity contours. For averaged vorticity contours, minimum and incremental levels of vorticity are ±1.5 and 1 l/s, respectively; for instantaneous contours, ±2.5 and 2.5 l/s.

takes on a distinctively different character than that of the present study.

Two representative distributions of instantaneous streamwise vorticity are given in Figs. 2c and 2d. In a very general sense, the overall features suggested by the averaged contours of Fig. 2b are detectable. The instantaneous structure is, however, highly distorted from one instant to the next. Not only the general form, but also the location of the vorticity concentrations exhibit substantial variations with time. It is evident that the averaging process, which gives rise to the image of Fig. 2b, smooths out even the concentrations of vorticity having substantial circulation; this smoothing is due to their random appearance from one image to the next, especially apparent for the region well above the leading edge (upper tip) of the fin, which is shown to be free of vorticity in the image of Fig. 2b. On the outboard side of the fin, the well-defined shear-layer region of Fig. 2b actually involves, in an instantaneous sense, discrete concentrations of vorticity. Similarly, on the inboard side, the large-scale vortex of the averaged images of Fig. 2b involves a number of discrete concentrations. Finally, the same observation holds for the negative concentration of countervorticity in Fig. 2b; it involves identifiable, but severely distorted concentrations of vorticity in the instantaneous images of Figs. 2c and 2d. The peak level of positive vorticity in Figs. 2c and 2d is 22.45 l/s; this compares with the peak positive vorticity 9.47 l/s in the averaged image of Fig. 2b, giving a ratio of instantaneous to peak vorticity of 2.37. The maximum values of instantaneous and averaged negative vorticity are −20.50 and −4.27 l/s, giving a ratio of 4.80.

B. Midregion of Fin

The averaged streamline pattern at a location corresponding to the midregion of the fin (see schematic region in Fig. 1) takes the form shown in Fig. 3a. The overall features of this sectional streamline pattern are similar to those of Fig. 2a, except for a tendency towards formation of an independent, large-scale vortical motion on the outboard side of the fin and a well-defined inward spiral of the streamlines located in the lower region of the image on the outboard side. On the other hand, the basic features of the outward-spiraling streamline pattern on the inboard side are very similar to those of Fig. 2a. The corresponding pattern of averaged vorticity given in Fig. 3b is again similar to its counterpart of Fig. 2b, except for the pronounced region of positive vorticity in the lower outboard region, which gives the inward-spiraling streamline pattern in that region. Particularly important, however, is the absence of the concentration of counter- (negative) vorticity in Fig. 3b, in comparison with the well-defined countervortex of Fig. 2b. Inspection of the instantaneous vorticity contours on the outboard side of the fin in Figs. 3c and 3d show that their form and location are highly inconsistent from one instant to the next. This large variation, along with the coexistence of a number of positive and negative concentrations of vorticity at each instant, produces cancellation of extreme vorticity levels during the averaging process in much the same manner as for Figs. 2c and 2d. The peak values of instantaneous positive vorticity in Figs. 3c and 3d are, respectively, 26.28 and 21.38 l/s, relative to the peak value of positive averaged vorticity of 7.45 l/s in Fig. 3b.

C. Trailing Region of Fin

Near the trailing end of the fin, defined by the plane of the laser sheet in Fig. 4, the flow structure is significantly different from those at upstream locations. Figure 4a indicates that there is no clearly defined spiral motion either on the inboard or outboard side, suggesting lower values of circulation in those regions. This loss of the spiraling streamline pattern occurs in conjunction with an upwash region directly beneath the lower edge of the fin. The corresponding contours of

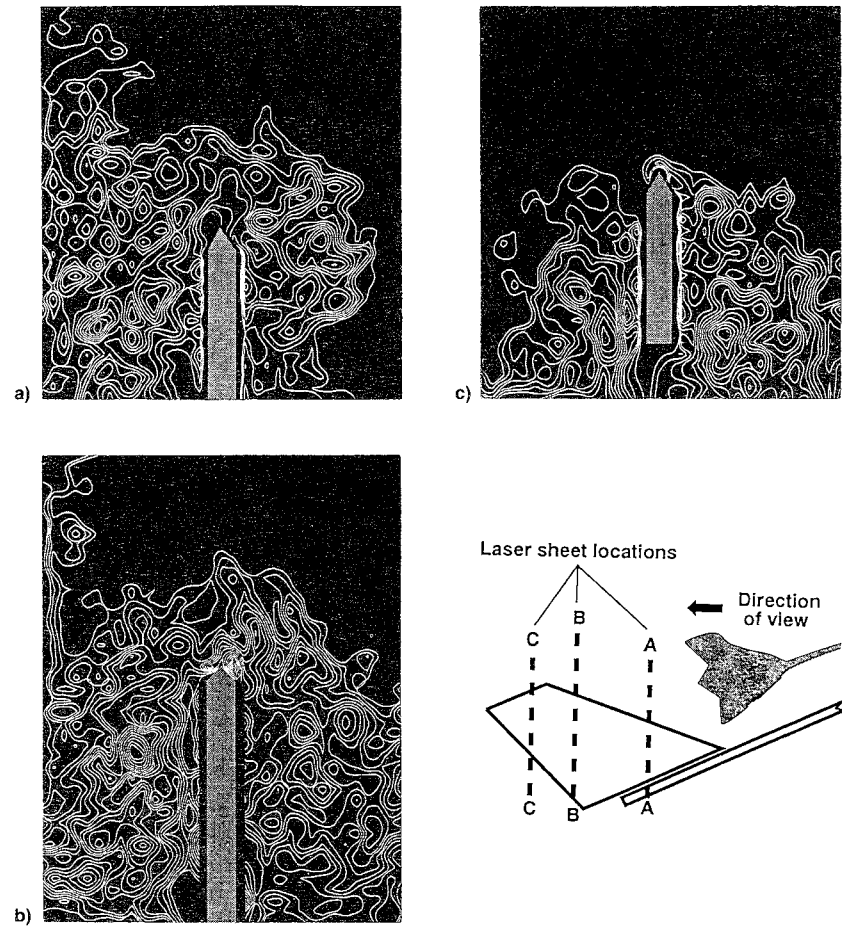

Fig. 5 Cross section of vortex–fin interaction showing contours of constant rms $\tilde{\omega}_{rms}$ at streamwise locations corresponding to a) leading, b) mid, and c) trailing regions of fin. For all plots, minimum and incremental levels of vorticity are 3 and 0.4 l/s, respectively.

averaged vorticity of Fig. 4b exhibit identifiable concentrations of vorticity on either side of the leading edge (apex) of the fin, a low-level concentration of vorticity on the outboard side and a broadly distributed region of concentrated vorticity on the inboard side. Moreover, in the upwash region beneath the lower edge, there is a pronounced concentration of negative vorticity.

In the instantaneous images of Figs. 4c and 4d the twin concentrations of vorticity at the leading-edge (upper tip) of the fin are readily apparent, as is the negative region of vorticity below the lower edge of the fin. Due to the particularly strong influence of the three dimensional efforts near the trailing edge of the fin, both positive and negative concentrations of vorticity are interspersed throughout the instantaneous images. The peak levels of positive and negative vorticity are 14.61 and −16.05 l/s, respectively, in comparison with corresponding levels of 8.04 and −4.48 l/s of the averaged image.

IV. Vorticity Fluctuations: Time-Averaged Representations

It is, of course, the time-dependent variation of the instantaneous vorticity that induces the surface pressure fluctuations on the fin. In order to quantitatively identify those regions of the flow that exhibit the largest amplitudes of fluctuating vorticity, the rms of $\tilde{\omega}_{rms}$ was evaluated over the entire plane of the crossflow. Each of the ith images employed for the averaging process corresponds to a vorticity distribution $\omega_i(y, z)$. Twenty such images were acquired at a time interval corresponding to C/U, which is an order of magnitude longer than the predominant frequency of the unsteady flow structure. The fluctuating vorticity was then determined by subtracting the mean vorticity of $\tilde{\omega}(y, z)$ of Fig. 2b from $\omega_i(y, z)$, represented, e.g., by the images of Figs. 2c and 2d. Finally, the rms of $\tilde{\omega}_{rms}$ was calculated according to

$$\tilde{\omega}_{rms} = \left\{ \frac{1}{N} \sum_{i=1}^{N} [\omega_i(y, z) - \tilde{\omega}(y, z)]^2 \right\}^{1/2} \quad (1)$$

For the representations of $\tilde{\omega}_{rms}$ shown in Fig. 5, a total of 20 instantaneous images were considered. For purposes of comparison, the minimum and incremental values of vorticity are the same in Figs. 5a–5c. Viewing images corresponding to Figs. 5a–5c, it is evident that particularly large gradients of vorticity fluctuation occur in the midregion of the fin, corresponding to Fig. 5b. Near the tip of the fin, the fluctuations are pronounced. At all streamwise locations, however, the fin is enveloped within a region of fluctuating vorticity of substantial level. In the trailing region, represented by Fig. 5c, levels of fluctuating vorticity are significantly reduced near the tip of the fin on the outboard side.

V. Concluding Remarks

Encounter of a broken-down vortex with a fin having a swept leading edge gives rise to several identifiable elements of the averaged and instantaneous flow patterns. The primary findings are as follows:

1) In the leading region of the fin, a countervortex, having a sense opposite to that of the incident vortex, is formed on the outboard side of the fin. Further downstream, at locations corresponding to the mid and trailing regions along the fin, this countervortex becomes less coherent and loses its identifiable structure.

2) On the far outboard side of the fin, the averaged vorticity takes the form of a relatively thin shear layer, which feeds into a large-scale, broadly distributed vortex on the inboard side. This basic pattern persists all the way to the trailing end of the fin, where only the averaged inboard vortex is identifiable.

3) All of the foregoing features of the averaged vortices are actually made up of an array of highly concentrated positive and negative vorticity, whose form and spatial location change substantially from one instant to the next. The maximum vorticity levels of these concentrations are typically a factor of 3–5 higher than those of corresponding regions of averaged vorticity.

4) Evaluation of distributions of rms fluctuating vorticity over the entire crossflow plane shows that the highest levels typically occur near the tip of the midregion of the fin.

Acknowledgments

The authors acknowledge the support of the Air Force Office of Scientific Research by Grants AFOSR-91-0055, F49620-93-1-0075, and F49620-94-1-0038.

References

[1]Mayori, A., and Rockwell, D., "Interaction of a Streamwise Vortex with a Thin Plate: A Source of Turbulent Buffeting," *AIAA Journal*, Vol. 32, No. 10, 1994, pp. 2022–2029.

[2]Shah, G. H., "Wind-Tunnel Investigation of Aerodynamic and Tail Buffet Characteristics of Leading-Edge Extension Modifications to the F/A-18," AIAA Paper 91-2889, Aug. 1991.

[3]Washburn, A. E., Jenkins, L. M., and Ferman, M. A., "Experimental Investigation of Vortex-Fin Interaction," AIAA Paper, Jan. 1993.

[4]Kiedaisch, J. W., and Acharya, M., "Interaction of Missile Tip Vortices with a Control Surface," AIAA Paper 94-0527, Jan. 1994.

[5]Lee, J. W., Cavone, A. A., and Suzuki, K. E., "Doppler Global Velocimetry Measurements of the Vortical Flow Above an F-18," AIAA Paper 93-0414, Jan. 1993.

[6]Canbazoglu, S., Lin, J.-C., Wolfe, S., and Rockwell, D., "Buffeting of Fin: Distortion of Incident Vortex," *AIAA Journal* (to be published).

[7]Rockwell, D., Magness, C., Robinson, O., Towfighi, J., Akin, O., Gu, W., and Corcoran, T., "Instantaneous Structure of Unsteady Separated Flows via Particle Image Velocimetry," Fluid Mechanics Labs., Rept. PI-1, Lehigh Univ., Bethlehem, PA, 1992.

[8]Rockwell, D., Magness, C., Towfighi, J., Akin, O., and Corcoran, T., "High-Image-Density PIV Using Laser Scanning Techniques," *Experiments in Fluids*, Vol. 14, 1993, pp. 181–192.

[9]Rockwell, D., and Lin, J.-C., "Quantitative Interpretation of Complex, Unsteady Flows via High-Image-Density Particle Image Velocimetry," SPIE International Symposium on Optics, Imaging and Instrumentation, San Diego, CA, July 1993.